2006

Elastic Wave Propagation in Sinusoidally Corrugated Waveguides

Sourav Banerjee
University of South Carolina, United States, banerjes@cec.sc.edu

Tribikram Kundu

Publication Info

Published in *The Journal of the Acoustical Society of America*, Volume 119, Issue 4, 2006, pages 2006-2017.

Banerjee, S. & Kundu, T. (2006). Elastic Wave Propagation in Sinusoidally Corrugated Waveguides. The Journal of the Acoustical Society of America, 119 (4), 2006-2017. http://dx.doi.org/10.1121/1.2172170

Elastic wave propagation in sinusoidally corrugated waveguides

Sourav Banerjee[a] and Tribikram Kundu[b]
Department of Civil Engineering and Engineering Mechanics, University of Arizona, Tucson, Arizona 85721

(Received 15 November 2005; revised 12 January 2006; accepted 13 January 2006)

The ultrasonic wave propagation in sinusoidally corrugated waveguides is studied in this paper. Periodically corrugated waveguides are gaining popularity in the field of vibration control and for designing structures with desired acoustic band gaps. Currently only numerical method (Boundary Element Method or Finite Element Method) based packages (e.g., PZFlex) are in principle capable of modeling ultrasonic fields in complex structures with rapid change of curvatures at the interfaces and boundaries but no analyses have been reported. However, the packages are very CPU intensive; it requires a huge amount of computation memory and time for its execution. In this paper a new semi-analytical technique called Distributed Point Source Method (DPSM) is used to model the ultrasonic field in sinusoidally corrugated waveguides immersed in water where the interface curvature changes rapidly. DPSM results are compared with analytical solutions. It is found that when a narrow ultrasonic beam hits the corrugation peaks at an angle, the wave propagates in the backward direction in waveguides with high corrugation depth. However, in waveguides with small corrugation the wave propagates in the forward direction. The forward and backward propagation phenomenon is found to be independent of the signal frequency and depends on the degree of corrugation. [DOI: 10.1121/1.2172170]

PACS number(s): 43.20.Fn, 43.20.El, 43.20.Bi [TDM] Pages: 2006–2017

I. INTRODUCTION

In recent years acoustic frequency filters are gaining popularity in the field of vibration and noise control and in acoustic bandgap analysis. The structures are being designed with periodic geometries to create acoustic bandgaps at desired frequencies. For the efficient design of such structures and correctly interpreting the experimental results with these structures, a complete understanding of elastic wave propagation in periodically corrugated structures is necessary. Another application of this study is in the nondestructive evaluation of different aerospace structures, components of integrated smart structures with nonplanar boundaries and civil structural components (rebars, pipelines, etc.).

The wave propagation analysis in structures with planar and curved boundaries has been the subject of numerous investigations for over five decades. The analytical solution of wave propagation in structures with nonplanar boundaries and interfaces has been the topic of investigation in the last three decades (Nayfeh *et al.*, 1978; Boström, 1983, 1989; Standström, 1986; Fokkemma, 1980; Glass and Maradudin, 1983; El-Bahrawy, 1994a, 1994b; Banerjee and Kundu, 2004; Declercq *et al.*, 2005). Stop bands and pass bands of the Rayleigh-Lamb symmetric modes in sinusoidally corrugated waveguides have been studied by El-Bahrawy (1994a). Only recently, generalized dispersion equations for periodically corrugated waveguides have been studied and solutions for both symmetric and antisymmetric modes in a sinusoidally corrugated waveguide have been presented (Banerjee and Kundu, 2006a).

In this paper a complete problem with a corrugated waveguide and two ultrasonic transducers is solved. The complete problem involves excitation of the corrugated plate by bounded acoustic beams that are generated by ultrasonic transducers of finite dimension [see Fig. 1(a)]. To solve this complete problem, appropriate modeling of the bounded acoustic beams in addition to the wave propagation modeling in corrugated plates is necessary. Modeling of ultrasonic and sonic fields generated by planar transducers of a finite dimension is one of the basic problems in textbooks (Rayleigh, 1965; Morse and Ingard,1968; Schmerr, 1998; Kundu, 2004). A good review of the earlier developments of the ultrasonic field modeling in front of a planar transducer can be found in Harris (1981). A list of the more recent developments in this field of research has been given by Sha *et al.* (2003). The pressure field in front of a planar transducer in homogeneous isotropic materials has been computed both in the time domain (Stepanishen, 1971; Harris, 1981; Jensen and Svendsen, 1992) and in the frequency domain (Ingenito and Cook, 1969; Lockwwod and Willette, 1973; Scarano *et al.*, 1985; Hah and Sung, 1992; Wu *et al.*, 1995; Lerch *et al.*, 1998). In addition to the ultrasonic field modeling in isotropic materials, progress has been made in the modeling of the ultrasonic radiation field in transversely isotropic and orthotropic media as well (Spies, 1994, 1995). Most of the abovementioned investigations are based on Huygen's principle, where the total field is obtained from the linear sum of point sources distributed over the transducer. The integral representation of this field is known as the Rayleigh-Sommerfield integral. Another technique based on the Gauss-Hermite beam model for ultrasonic field modeling in anisotropic ma-

[a]Electronic mail: sourav@email.arizona.edu
[b]Corresponding author: Tribikram Kundu, Department of Civil Engineering and Engineering Mechanics, University of Arizona, Tucson, Arizona 85721. Telephone: (520) 621 6573; electronic mail: tkundu@email.arizona.edu

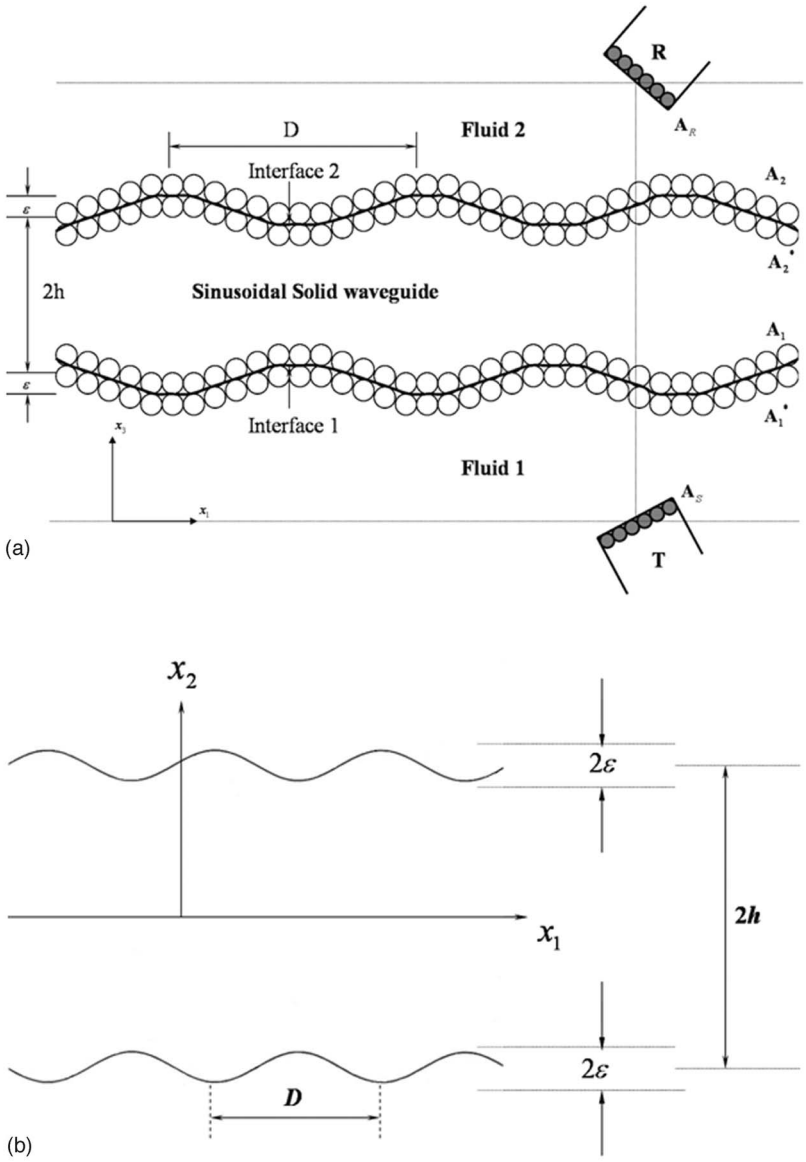

FIG. 1. (a) Sinusoidally corrugated waveguide between two transducers—geometry for the DPSM analysis. (b) Sinusoidally corrugated waveguide showing different parameters considered for the analytical solution.

terials with a paraxial approximation was proposed by Newberry and Thompson (1989). Since numerical integration is a time-consuming operation, Wen and Breazeale (1988) proposed an alternative approach. They computed the total field by superimposing a number of Gaussian beam solutions. They have shown that by superimposing only ten Gaussian solutions, the field radiated by a circular piston transducer can be modeled. Schmerr (2000) followed this approach to compute the ultrasonic field near a curved fluid-solid interface. Later Spies (1999) and Schmerr *et al.* (2003) extended this technique to a homogeneous anisotropic solid and water immersed anisotropic solid, respectively. Although a significant progress has been made in the ultrasonic field modeling in a homogeneous medium, the effect of curved interface with gradually varying curvature near an ultrasonic transducer of finite dimension has not been studied extensively yet. Recently Schmerr (2000) and Schmerr *et al.* (2003) studied the ultrasonic field near a fluid-solid curved interface. Spies (2004) studied the effect of the interface on the ultrasonic wave propagation in an inhomogeneous anisotropic medium with the farfield approximation. These investigators followed multi-Gaussian beam modeling approach. Although this technique has some computational advantage it also has a number of limitations similar to those of other paraxial models. For example, it cannot correctly model the critical reflection phenomenon; it cannot model a transmitted beam at an interface near grazing incidence. This technique also fails if the interface has different curvatures (gradually varying curvature), or when the radius of curvature of the transducer is small, as observed in acoustic microscopy experiments with its tightly focused lens. A detail description of the limitations of the multi-Gaussian paraxial models can be found in Schmerr *et al.* (2003).

The technique based on the DPSM (Distributed Point Source Method), proposed by Placko and Kundu (2001, 2004) avoids the above-mentioned limitations and does not require any farfield approximation. In this technique, one layer of point sources are distributed near the transducer face and two layers are placed near the interface. The advantage of the DPSM technique is that it not only avoids the paraxial

approximation it also does not require any ray tracing. The DPSM technique can handle complex geometries of the interface and the transducer. All methods developed before DPSM for the ultrasonic field radiation modeling near an interface requires ray tracing. The ray tracing technique becomes cumbersome in the presence of multiple interfaces while such geometries can be easily modeled by the DPSM technique (Banerjee, Kundu, and Placko, 2006).

The DPSM technique for ultrasonic field modeling was first developed by Placko and Kundu (2001). They successfully used this technique to model ultrasonic fields in a homogeneous fluid, and in a nonhomogeneous fluid with one interface (Lee *et al.*, 2002; Placko *et al.*, 2002) as well as multiple interfaces (Banerjee, 2005). The interaction between two transducers for different transducer arrangements and source strengths, placed in a homogeneous fluid, has been studied by Ahmad *et al.* (2003). The scattered ultrasonic field generated by a solid scatterer of finite dimension placed in a homogeneous fluid has also been modeled by the DPSM technique (Placko *et al.*, 2003). Recently the method has been extended to model the phased array transducers (Ahmad *et al.*, 2005). All these works modeled the ultrasonic field in a fluid medium. Only recently, the method has been extended to model the ultrasonic fields inside solid structures with planar boundaries (Banerjee and Kundu, 2006b). In the current paper the ultrasonic field in a sinusoidally corrugated waveguide has been modeled by the DPSM technique. The details of this modeling, as described in the subsequent sections, are quite challenging because of the continuous variations of the curvature of the fluid-solid interface. Numerical results for corrugated waveguides showing forward and backward propagations of guided waves depending on the degree of corrugation are reported here for the first time in the literature.

II. THEORY

A. Problem geometry

A symmetrically corrugated sinusoidal waveguide is considered. On two sides of the waveguide Fluid 1 and Fluid 2 are used as the coupling fluids that transmit ultrasonic waves from the ultrasonic transducers to the waveguide [see Fig. 1(a)]. To model the ultrasonic field inside the waveguide and the fluid, the DPSM technique (Placko *et al.*, 2001; Lee *et al.*, 2002; Ahmad *et al.*, 2005) is employed. Following the basics of the DPSM technique, four sets of point sources are distributed on both sides of the waveguide, as shown in Fig. 1(a). Point sources are also distributed behind the transducer faces. Transducer sources are denoted as $\mathbf{A}_S$ and $\mathbf{A}_R$ in Fig. 1(a). $\mathbf{A}_S, \mathbf{A}_R, \mathbf{A}_1, \mathbf{A}_2, \mathbf{A}_1^*$, and $\mathbf{A}_2^*$ are the source strength vectors for the sources distributed near the transducer surfaces and two interfaces [see Fig. 1(a)]. The period of corrugation of the sinusoidal waveguide is D and the depth of corrugation is equal to ε [see Fig. 1(b)].

B. Matrix formulation

The particle velocity and pressure in fluids at the interfaces can be expressed in matrix form (Kundu, 2004). Let $T1$ and $T2$ be two different sets of target points in the fluid below and above the Interfaces 1 and 2, respectively. The velocity at the target points can be written as

$$\mathbf{V}_{T1} = \mathbf{M}_{(T1)S}\mathbf{A}_S + \mathbf{M}_{(T1)1}\mathbf{A}_1, \tag{1}$$

$$\mathbf{V}_{T2} = \mathbf{M}_{(T2)R}\mathbf{A}_R + \mathbf{M}_{(T2)2^*}\mathbf{A}_2^*. \tag{2}$$

Similarly, the pressure fields at the target points are

$$\mathbf{PR}_{T1} = \mathbf{PR}_{T1}^s + \mathbf{PR}_{T1}^1 = \mathbf{Q}_{(T1)S}\mathbf{A}_S + \mathbf{Q}_{(T1)1}\mathbf{A}_1, \tag{3}$$

$$\mathbf{PR}_{T2} = \mathbf{PR}_{T2}^s + \mathbf{PR}_{T2}^{2^*} = \mathbf{Q}_{(T2)R}\mathbf{A}_R + \mathbf{Q}_{(T2)2^*}\mathbf{A}_2^*. \tag{4}$$

Elements of the matrices written in Eqs. (1)–(4) are given in Kundu (2004).

Boundary surfaces of the sinusoidal waveguide are nonplanar. At every point of the interface, normal stress and normal displacement are to be defined to satisfy the continuity conditions across the interface. The direction cosine of the sinusoidal waveguide at any point on the surface can be defined as $n=(n_1e_1+n_2e_2)$. Projections of unit normal (n) on x_1 and x_2 axes are given in Eqs. (5) and (6), respectively,

$$n_1 = \frac{\frac{2\pi\varepsilon}{D}\sin\left(\frac{2\pi x_1}{D}\right)}{\left[\left(\frac{2\pi\varepsilon}{D}\right)^2 \sin^2\left(\frac{2\pi x_1}{D}\right) + 1\right]^{1/2}}, \tag{5}$$

$$n_2 = \frac{1}{\left[\left(\frac{2\pi\varepsilon}{D}\right)^2 \sin^2\left(\frac{2\pi x_1}{D}\right) + 1\right]^{1/2}}. \tag{6}$$

Point sources needed for modeling isotropic solids are different from those used for fluid modeling. Every point source for the solid modeling has three different force components in three mutually perpendicular directions. For a point source acting at **y** in an isotropic solid, the stresses developed at point **x** have been expressed by Banerjee (2005) and Banerjee and Kundu (2006b). Assuming a point force acting along the x_j direction, stresses at point **x** on the boundary of the sinusoidal waveguide can be written as

$$\boldsymbol{\sigma}^j = \begin{bmatrix} \sigma_{11}^j & \sigma_{12}^j & \sigma_{13}^j \\ \sigma_{21}^j & \sigma_{22}^j & \sigma_{23}^j \\ \sigma_{31}^j & \sigma_{32}^j & \sigma_{33}^j \end{bmatrix}. \tag{7}$$

The transformation matrix at point **x** is

$$\mathbf{T} = \begin{bmatrix} n_2 & -n_1 & 0 \\ n_1 & n_2 & 0 \\ 0 & 0 & 1 \end{bmatrix}. \tag{8}$$

Therefore, transformed stresses at point **x** is

$$\underline{\boldsymbol{\sigma}'^{j}} = \mathbf{T}\boldsymbol{\sigma}^{j}\mathbf{T}^{T} = \begin{bmatrix} n_2 & -n_1 & 0 \\ n_1 & n_2 & 0 \\ 0 & 0 & 1 \end{bmatrix} \begin{bmatrix} \sigma_{11}^{j} & \sigma_{12}^{j} & \sigma_{13}^{j} \\ \sigma_{21}^{j} & \sigma_{22}^{j} & \sigma_{23}^{j} \\ \sigma_{31}^{j} & \sigma_{32}^{j} & \sigma_{33}^{j} \end{bmatrix} \times \begin{bmatrix} n_2 & n_1 & 0 \\ -n_1 & n_2 & 0 \\ 0 & 0 & 1 \end{bmatrix} = \begin{bmatrix} \sigma_{11}'^{j} & \sigma_{12}'^{j} & \sigma_{13}'^{j} \\ \sigma_{21}'^{j} & \sigma_{22}'^{j} & \sigma_{23}'^{j} \\ \sigma_{31}'^{j} & \sigma_{32}'^{j} & \sigma_{33}'^{j} \end{bmatrix}. \quad (9)$$

To define the boundary conditions at point **x**, one normal stress, perpendicular to the sinusoidal boundary surface and two shear stresses, parallel to the boundary surface are needed. Considering a set of M point sources distributed on the sinusoidal surface, the normal stress and the shear stress components can be defined as

$$S_{22}' = \sum_{m=1}^{M} [(\sigma_{22}'^{1})^m P_1^m + (\sigma_{22}'^{2})^m P_2^m + (\sigma_{22}'^{3})^m P_3^m] = \sum_{m=1}^{M} \underline{\mathbf{s}_{22}'}^m \left(\frac{\mathbf{P}}{4\pi}\right)^m, \quad (10)$$

$$S_{21}' = \sum_{m=1}^{M} [(\sigma_{21}'^{1})^m P_1^m + (\sigma_{21}'^{2})^m P_2^m + (\sigma_{21}'^{3})^m P_3^m] = \sum_{m=1}^{M} \underline{\mathbf{s}_{21}'}^m \left(\frac{\mathbf{P}}{4\pi}\right)^m, \quad (11)$$

$$S_{23}' = \sum_{m=1}^{M} [(\sigma_{23}'^{1})^m P_1^m + (\sigma_{23}'^{2})^m P_2^m + (\sigma_{23}'^{3})^m P_3^m] = \sum_{m=1}^{M} \underline{\mathbf{s}_{23}'}^m \left(\frac{\mathbf{P}}{4\pi}\right)^m. \quad (12)$$

Displacements at point **x** generated by a point source acting at point **y** in an isotropic solid can be obtained from Mal and Singh (1991). The displacements at **x** due to the point force acting along the x_j direction are denoted as G_{1j}, G_{2j}, and G_{3j}. Considering the same point force along the x_j direction, the normal displacement of the sinusoidal solid surface at **x** can be written as

$$u_n^j = G_{1j}n_1 + G_{2j}n_2. \quad (13)$$

Considering a set of M point sources distributed on the interface, the normal displacement at point **x** on the sinusoidal surface can be written as

$$\underline{un} = \sum_{m=1}^{M} [(G_{11}n_1 + G_{21}n_2)^m P_1^m + (G_{12}n_1 + G_{22}n_2)^m P_2^m + (G_{13}n_1 + G_{23}n_2)^m P_3^m] = \sum_{m=1}^{M} \underline{\mathbf{Gn}}^m \mathbf{P}^m. \quad (14)$$

Let T be a set of target points in the solid. Normal displacements at these points (T) on the sinusoidal surface can be written in the following form:

$$\underline{\mathbf{un}}_T = \mathbf{DSn}_{T1^*}\mathbf{A}_1^* + \mathbf{DSn}_{T2}\mathbf{A}_2. \quad (15)$$

Similarly transformed normal stress and shear stresses at the target points (T) on the sinusoidal surface can be written as

$$\mathbf{s22}_T' = \mathbf{S22}_{T1^*}'\mathbf{A}_1^* + \mathbf{S22}_{T2}'\mathbf{A}_2, \quad (16a)$$

$$\mathbf{s21}_T' = \mathbf{S21}_{T1^*}'\mathbf{A}_1^* + \mathbf{S21}_{T2}'\mathbf{A}_2, \quad (16b)$$

$$\mathbf{s23}_T' = \mathbf{S23}_{T1^*}'\mathbf{A}_1^* + \mathbf{S23}_{T2}'\mathbf{A}_2. \quad (16c)$$

Matrices $\mathbf{DSn}_{TS}$ and $\mathbf{S22}_{TS}'$ are given in the Appendix [see Eqs. (A1) and (A2)]. Similarly $\mathbf{S21}_{TS}'$ and $\mathbf{S23}_{TS}'$ can be expressed. Subscripts T and S denote sets of target and source points, respectively.

In a fluid medium, the displacement components at point **x** generated by a point source at **y** are expressed as follows (Banerjee, 2005):

$$u_1 = \frac{1}{4\pi\rho\omega^2}\left(\frac{1}{r}ik_f R_1 e^{ik_f r} - \frac{e^{ik_f r}}{r^2}R_1\right), \quad (17)$$

$$u_2 = \frac{1}{4\pi\rho\omega^2}\left(\frac{1}{r}ik_f R_2 e^{ik_f r} - \frac{e^{ik_f r}}{r^2}R_2\right), \quad (18)$$

$$u_3 = \frac{1}{4\pi\rho\omega^2}\left(\frac{1}{r}ik_f R_3 e^{ik_f r} - \frac{e^{ik_f r}}{r^2}R_3\right), \quad (19)$$

where $R_j = (x_j - y_j)/r$, j takes values 1, 2, and 3.

Using the direction cosines (n_i) of the normal vector to the corrugated surface, the displacement component normal to the corrugated interface at point **x** can be written as

$$u_{fn} = u_1 n_1 + u_2 n_2. \quad (20)$$

Following the same rule in presence of transducers [see Fig. 1(a)], the displacement of the fluid at Interfaces 1 and 2 can be written as

$$\underline{\mathbf{Un}}_{I1} = [(\mathbf{DF2}_{(I1)S})n_2 + (\mathbf{DF1}_{(I1)S})n_1]\mathbf{A}_S + [(\mathbf{DF2}_{(I1)1})n_2 + (\mathbf{DF1}_{(I1)1})n_1]\mathbf{A}_1, \quad (21)$$

$$\underline{\mathbf{Un}}_{I2} = [(\mathbf{DF2}_{(I2)R})n_2 + (\mathbf{DF1}_{(I2)R})n_1]\mathbf{A}_R + [(\mathbf{DF2}_{(I2)2^*})n_2 + (\mathbf{DF1}_{(I2)2^*})n_1]\mathbf{A}_2^*, \quad (22)$$

or

$$\underline{\mathbf{Un}}_{I1} = \mathbf{DFn}_{(I1)S}\mathbf{A}_S + \mathbf{DFn}_{(I1)1}\mathbf{A}_1, \quad (23)$$

$$\underline{\mathbf{Un}}_{I2} = \mathbf{DFn}_{(I2)R}\mathbf{A}_R + \mathbf{DFn}_{(I2)2^*}\mathbf{A}_2^*. \quad (24)$$

Matrix $\mathbf{DFn}_{TS}$ is given in the Appendix [Eq. (A3)], where T and S denote sets of target and source points, respectively.

Let us consider a set of target points on "Interface 1" (then the set of target points will be denoted as $I1$) and the transformed normal stress and shear stress matrices for the referenced target points can be written as

$$\mathbf{s22}_{I1}' = \mathbf{S22}_{I11^*}'\mathbf{A}_1^* + \mathbf{S22}_{I12}'\mathbf{A}_2, \quad (25a)$$

$$\mathbf{s21}_{I1}' = \mathbf{S21}_{I11^*}'\mathbf{A}_1^* + \mathbf{S21}_{I12}'\mathbf{A}_2, \quad (25b)$$

$$\mathbf{s23}'_{I1} = \mathbf{S23}'_{I11^*}\mathbf{A}_1^* + \mathbf{S23}'_{I12}\mathbf{A}_2. \tag{25c}$$

Similarly, on Interface 2, the set of target points are denoted as $I2$ and the transformed normal and shear stresses on the sinusoidal surface can be written as

$$\mathbf{s22}'_{I2} = \mathbf{S22}'_{I21^*}\mathbf{A}_1^* + \mathbf{S22}'_{I22}\mathbf{A}_2, \tag{26a}$$

$$\mathbf{s21}'_{I2} = \mathbf{S21}'_{I21^*}\mathbf{A}_1^* + \mathbf{S21}'_{I22}\mathbf{A}_2, \tag{26b}$$

$$\mathbf{s23}'_{I2} = \mathbf{S23}'_{I21^*}\mathbf{A}_1^* + \mathbf{S23}'_{I22}\mathbf{A}_2. \tag{26c}$$

Inside the solid at interfaces $I1$ and $I2$, the normal displacements can be written as

$$\underline{\mathbf{un}}_{I1} = \mathbf{DSn}_{(I1)1^*}\mathbf{A}_1^* + \mathbf{DSn}_{(I1)2}\mathbf{A}_2, \tag{27}$$

$$\underline{\mathbf{un}}_{I2} = \mathbf{DSn}_{(I2)1^*}\mathbf{A}_1^* + \mathbf{DSn}_{(I2)2}\mathbf{A}_2. \tag{28}$$

C. Boundary and continuity conditions

Across the fluid-solid interface the displacement component normal to the interface should be continuous. Also, at the interface, the transformed normal stress ($\mathbf{s22}'$) in the solid and pressure in the fluid should be continuous. Whereas, the shear stresses at the interface must vanish. Let the normal velocities at the transducer faces be $\mathbf{V}_{S0}$ and $\mathbf{V}_{R0}$, for the lower and upper transducers, respectively. The boundary conditions at the transducer faces are

$$\mathbf{M}_{SS}\mathbf{A}_S + \mathbf{M}_{S1}\mathbf{A}_1 = \mathbf{V}_{S0}, \tag{29}$$

$$\mathbf{M}_{R2^*}\mathbf{A}_2^* + \mathbf{M}_{RR}\mathbf{A}_R = \mathbf{V}_{R0}. \tag{30}$$

At the interfaces, from the continuity of the normal stress,

$$\mathbf{Q}_{1S}\mathbf{A}_S + \mathbf{Q}_{11}\mathbf{A}_1 = -\mathbf{S22}'_{11^*}\mathbf{A}_1^* - \mathbf{S22}'_{12}\mathbf{A}_2, \tag{31}$$

$$\mathbf{Q}_{22^*}\mathbf{A}_2^* + \mathbf{Q}_{2R}\mathbf{A}_R = -\mathbf{S22}'_{21^*}\mathbf{A}_1^* - \mathbf{S22}'_{22}\mathbf{A}_2. \tag{32}$$

Continuity of the normal displacement gives

$$\mathbf{DFn}_{1S}\mathbf{A}_S + \mathbf{DFn}_{11}\mathbf{A}_1 = \mathbf{DSn}_{11^*}\mathbf{A}_1^* + \mathbf{DSn}_{12}\mathbf{A}_2, \tag{33}$$

$$\mathbf{DFn}_{22^*}\mathbf{A}_2^* + \mathbf{DFn}_{2R}\mathbf{A}_R = \mathbf{DSn}_{21^*}\mathbf{A}_1^* + \mathbf{DSn}_{22}\mathbf{A}_2, \tag{34}$$

and from the vanishing shear stress condition at the fluid-solid interface,

$$\mathbf{S21}'_{11^*}\mathbf{A}_1^* + \mathbf{S21}'_{12}\mathbf{A}_2 = 0, \tag{35}$$

$$\mathbf{S23}'_{11^*}\mathbf{A}_1^* + \mathbf{S23}'_{12}\mathbf{A}_2 = 0. \tag{36}$$

Equations (29)–(36) can be written in matrix form,

$$\begin{bmatrix}
\mathbf{M}_{SS} & \mathbf{M}_{S1} & \mathbf{0} & \mathbf{0} & \mathbf{0} & \mathbf{0} \\
\mathbf{Q}_{1S} & \mathbf{Q}_{11} & \mathbf{S22}'_{11^*} & \mathbf{S22}'_{12} & \mathbf{0} & \mathbf{0} \\
\mathbf{DFn}_{1S} & \mathbf{DFn}_{11} & -\mathbf{DSn}_{11^*} & -\mathbf{DSn}_{12} & \mathbf{0} & \mathbf{0} \\
\mathbf{0} & \mathbf{0} & \mathbf{S21}'_{11^*} & \mathbf{S21}'_{12} & \mathbf{0} & \mathbf{0} \\
\mathbf{0} & \mathbf{0} & \mathbf{S23}'_{11^*} & \mathbf{S23}'_{12} & \mathbf{0} & \mathbf{0} \\
\mathbf{0} & \mathbf{0} & \mathbf{S23}'_{21^*} & \mathbf{S23}'_{22} & \mathbf{0} & \mathbf{0} \\
\mathbf{0} & \mathbf{0} & \mathbf{S21}'_{21^*} & \mathbf{S21}'_{22} & \mathbf{0} & \mathbf{0} \\
\mathbf{0} & \mathbf{0} & \mathbf{S22}'_{21^*} & \mathbf{S22}'_{22} & \mathbf{Q}_{22^*} & \mathbf{Q}_{2R} \\
\mathbf{0} & \mathbf{0} & -\mathbf{DSn}_{21^*} & -\mathbf{DSn}_{22} & \mathbf{DFn}_{22^*} & \mathbf{DFn}_{2R} \\
\mathbf{0} & \mathbf{0} & \mathbf{0} & \mathbf{0} & \mathbf{M}_{R2^*} & \mathbf{M}_{RR}
\end{bmatrix}_{(2N+8M)x(2N+8M)}$$

$$, \quad \begin{Bmatrix} \mathbf{A}_S \\ \mathbf{A}_1 \\ \mathbf{A}_1^* \\ \mathbf{A}_2 \\ \mathbf{A}_2^* \\ \mathbf{A}_R \end{Bmatrix}_{(2N+8M)} = \begin{Bmatrix} \mathbf{V}_{S0} \\ \mathbf{0} \\ \mathbf{0} \\ \mathbf{0} \\ \mathbf{0} \\ \mathbf{0} \\ \mathbf{0} \\ \mathbf{V}_{R0} \end{Bmatrix}_{(2N+8M)} , \tag{37}$$

or

$$[\underline{\mathbf{MT}}]\{\mathbf{\Omega}\} = \{\mathbf{V}\}. \tag{38}$$

D. Solution

The vector of source strengths of the complete system can be obtained from Eq. (38) by taking inverse of $[\underline{\mathbf{MT}}]$ and multiplying it with the vector $\{\mathbf{V}\}$,

$$\{\mathbf{\Omega}\} = [\underline{\mathbf{MT}}]^{-1}\{\mathbf{V}\}. \tag{39}$$

After calculating the source strengths, the pressure, velocity, stress, and displacement values at any point can be obtained.

E. Analytical solution of wave propagation in sinusoidally corrugated waveguide

The analytical solution for the complete problem geometry including the waveguide and two transducers as shown in Fig. 1(a) is not available. However, the problem of guided wave propagation in a corrugated plate as shown in Fig. 1(b)

can be solved analytically. Wave propagation in corrugated waveguides with small corrugation, where the perturbation method can be applied, was first studied by Nayfeh *et al.* (1978). This solution cannot be used in many practical applications when the corrugation height is not necessarily small in comparison to the plate thickness. The analysis of wave propagation in electromagnetic waveguides with a high degree of corrugation was studied by Boström (1983). Later, Standström (1986) discussed stop bands in sinusoidally corrugated waveguides by applying the null-field approach, developed by Waterman (1975). Standström (1987) compared different techniques for the corrugated plate analysis.

The elastic wave propagation analysis near sinusoidally corrugated fluid-solid interface by the modal superposition technique has been discussed by Fokkemma (1980). Although a number of researchers have studied the electromagnetic wave propagation near surface grating and in corrugated waveguides, not many investigators have studied the problem of elastic wave propagation in corrugated plates. The problem of elastic wave propagation in a sinusoidally corrugated waveguide has been considered by El-Bahrawy (1994a) for only symmetric Rayleigh-Lamb modes. A classical modal technique was adopted for this analysis. In El-Bahrawy's study the dispersion equation was developed for only symmetric modes. Stop bands and pass bands of the symmetric modes were studied extensively by El-Bahrawy.

In this paper the analytical solution is adopted from El-Bahrawy's (1994a) work. The dispersion relation for the symmetric modes in a sinusoidally corrugated waveguide is presented in Eq. (40). The parameters (ε, D, h) used in the following equations are defined in Fig. 1(b):

$$T_{ij}\alpha_j = 0. \tag{40a}$$

Therefore, for nontrivial solutions of α_j,

$$\mathrm{Det}[T] = 0, \tag{40b}$$

where

$$\begin{aligned}
T_{1n1m} &= -i\frac{D}{2}\left(\frac{k_n}{\beta_n}\right)(i^{n-m}e^{ih\beta_n} - i^{m-n}e^{-ih\beta_n}) \\
&\quad\times\left[\left(\frac{4(n-m)\pi}{D}\right)k_n + 2\beta_n^2 - k_s^2\right]J_{n-m}(\varepsilon\beta_n), \\
T_{1n2m} &= -(i^{n-m}e^{ih\eta_n} - i^{m-n}e^{-ih\eta_n}) \\
&\quad\times\left[\left(\frac{(n-m)\pi}{\eta_n}\right)(k_s^2 - 2\eta_n^2) + Dk_n\eta_n\right]J_{n-m}(\varepsilon\beta_n), \\
T_{2n1m} &= -k_n(i^{n-m}e^{ih\beta_n} + i^{m-n}e^{-ih\beta_n}) \\
&\quad\times\left[\left(\frac{(n-m)\pi}{\beta_n^2}\right)(k_s^2 - 2\beta_n^2) + Dk_n\right]J_{n-m}(\varepsilon\beta_n), \\
T_{2n2m} &= -(i^{n-m}e^{ih\eta_n} + i^{m-n}e^{-ih\eta_n}) \\
&\quad\times\left(-\frac{D}{2}(k_s^2 - 2\beta_n^2) + 2\pi(n-m)k_n\right)J_{n-m}(\varepsilon\beta_n).
\end{aligned} \tag{40c}$$

In the above equations, if n and m take values 1, 2, 3, …, p, then i and j take values 1, 2, 3, …, 2IpI, (2IpI+1).

The displacement function can be written as

$$u_k = w_{kj}\alpha_j, \tag{41}$$

where k takes values 1, 2, and 3.

The displacement functions have been given by El-Bahrawy (1994a). Equation (40) is solved for a particular frequency and the eigenvectors corresponding to the wave number solutions are calculated. The eigenvector solutions are substituted in Eq. (41) to get displacement mode shape in the waveguide for a specific mode.

The above analytical solution is for the plane wave propagation in the waveguide. However, the wave field in the waveguide for the DPSM modeling is generated by two bounded acoustic beams. Therefore, perfect matching between the DPSM generated results and the analytical mode shapes is not expected. Only a qualitative comparison between these two results is presented in the following section. The symmetric transducer placement in the DPSM formulation generates only the symmetric modes in the waveguide. Hence, only the symmetric mode solutions of the analytical formulation are compared with the DPSM results.

TABLE I. Waveguide geometry [see Fig. 1(b)].

	$2h$	ε	D	ε/D
Waveguide 1	10	0.5	10	0.05
Waveguide 2	10	1	10	0.1
Waveguide 3	10	1.5	10	0.15
Waveguide 4	10	2	10	0.2

III. NUMERICAL IMPLEMENTATION

MATLAB 7.1 R-14 and Lapack library functions are used to generate the numerical results based on the formulation presented above. The numerical results are presented for the corrugated aluminum waveguides with Lamé constants λ and μ equal to 54.55 and 24.95 GPa, respectively, and density equal to 2.7 gm/cm^3. P-wave and S-wave speeds (c_p =6220 m/s and c_s=3040 m/s) in the material are obtained from the above elastic constants. Four different waveguides are considered in the analysis. Dimensions of the waveguides are presented in Table I. Comparisons between DPSM and analytical solutions are presented for Waveguide 2.

Equation (40) is solved numerically for two different frequencies from the pass band frequencies [El-Bahrway (1994a)]. The ultrasonic fields for these frequencies are also generated by the DPSM technique. The absolute values of the horizontal and vertical displacement components computed by these two methods are presented in Figs. 2(a) and 2(b), respectively. The plots show the displacement variations along the plate thickness. The displacement fields are normalized with respect to the horizontal displacement at x_2=0 [see Fig. 1(b)]. For comparison purposes the displacement field from the DPSM formulation is generated away from the transducers to capture the propagating guided wave modes away from the zone affected by the striking ultrasonic beams. The displacement fields corresponding to the first two symmetric modes generated from Eq. (41) are multiplied by

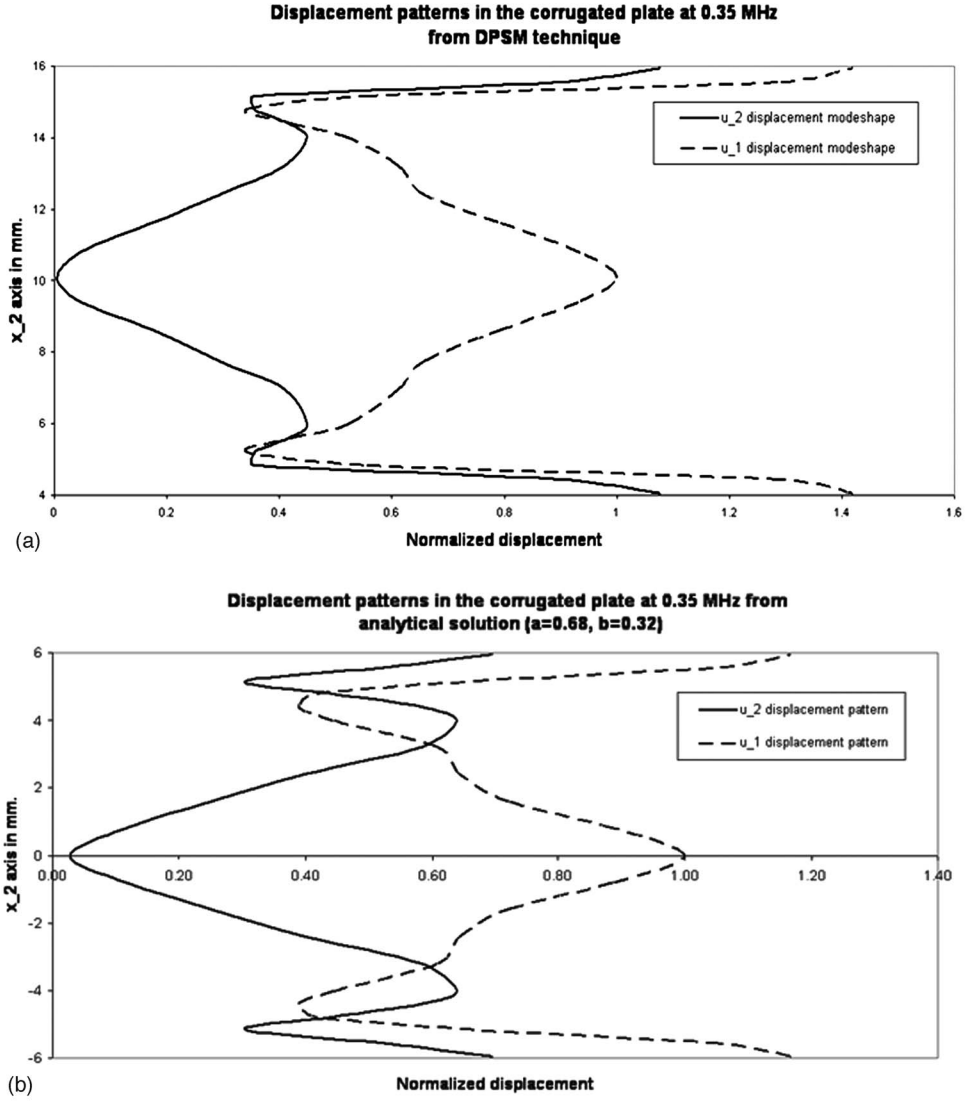

FIG. 2. Horizontal and vertical displacement variations at 0.35 MHz along the plate thickness obtained by (a) DPSM and (b) analytical solution techniques.

two weight factors and added to approximately match the DPSM results. The weighted displacement field is calculated as

$$u_i = w_1 u_i^1 + w_2 u_i^2, \tag{42}$$

where u_i^1 and u_i^2 are displacement components along the x_i direction generated by the fundamental and first higher symmetric modes, respectively. Results presented in Fig. 2(b) are generated with $w_1=0.68$ and $w_2=0.32$. Clearly, the DPSM results are qualitatively in good agreement with the analytical solution.

Ultrasonic fields in four different waveguides (see Table I) are generated by the DPSM technique. A normal incidence of the ultrasonic beam on a corrugation peak of the waveguide is considered first and then the transducers are inclined at two different angles. Results for three different orientations of the transducers are presented. Figure 3 shows different transducer orientations. The transducer frequency is set at 1 MHz. Figures 4 and 5 show the horizontal (u_1) and vertical (u_2) displacement fields, respectively, inside the waveguides. In these two figures the displacement fields are presented for Waveguides 2, 3, and 4 (see Table I for their dimensions). Figures 4(a), 4(b), and 4(c) show the u_1 displacement for normal incidence [transducer orientation is shown in Fig. 5(a)] in Waveguides 2, 3, and 4, respectively. Figures 4(d),

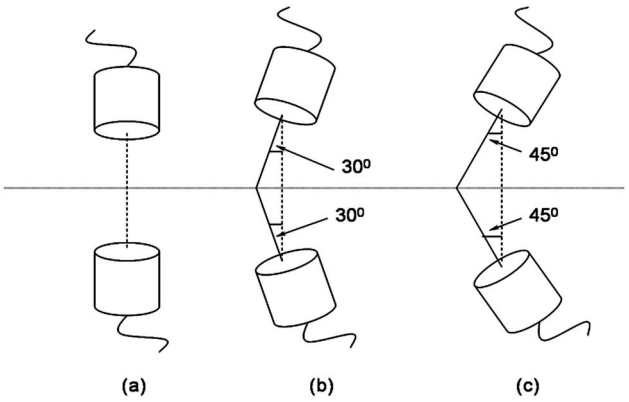

FIG. 3. Transducer orientations (a) Orientation—I: Normal Incidence. (b) Orientation—II: 30° inclination. (c) Orientation—III: 45° inclination.

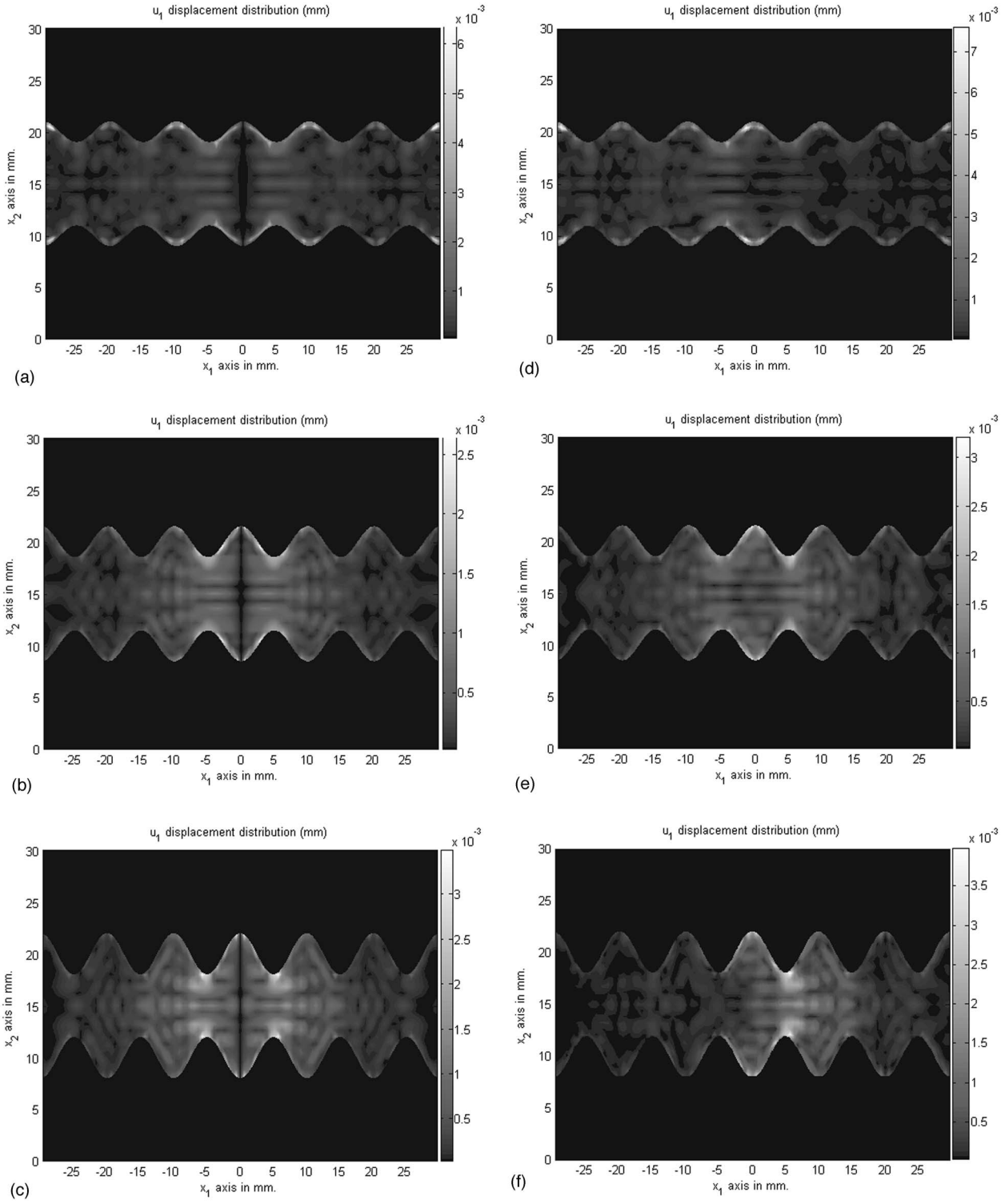

FIG. 4. Horizontal displacement fields in three different corrugated waveguides (2, 3, and 4) for two different angles of strike (0° and 30°). (a) in Waveguide 2 for normal incidence, (b) in Waveguide 3 for normal incidence, (c) in Waveguide 4 for normal incidence, (d) in Waveguide 2 for a 30° inclination angle, (e) in Waveguide 3 for a 30° inclination angle, (f) in Waveguide 4 for a 30° inclination angle. However, for inclined incidence, more energy is observed in the backward direction ($x>0$) in Fig. 4(f) (large corrugation) while the opposite trend is noticed in Fig. 4(e) (small corrugation). Table I gives waveguide dimensions.

4(e), and 4(f) show the u_1 displacement for 30° striking angle (transducer orientation is shown in Fig. 3(b)) in Waveguides 2, 3, and 4, respectively. Similarly, Figs. 5(a), 5(b), and 5(c) show the u_2 displacement for normal incidence in Waveguides 2, 3, and 4, respectively, and Figs. 5(d), 5(e), and 5(f) show the u_2 displacement for a 30° striking angle in Waveguides 2, 3, and 4, respectively. It can be seen from Figs. 4 and 5 that the ultrasonic waves in Waveguide 2 [Figs. 4(d) and 5(d)] propagate in the forward direction, or in other words, in the same direction as the horizontal component of

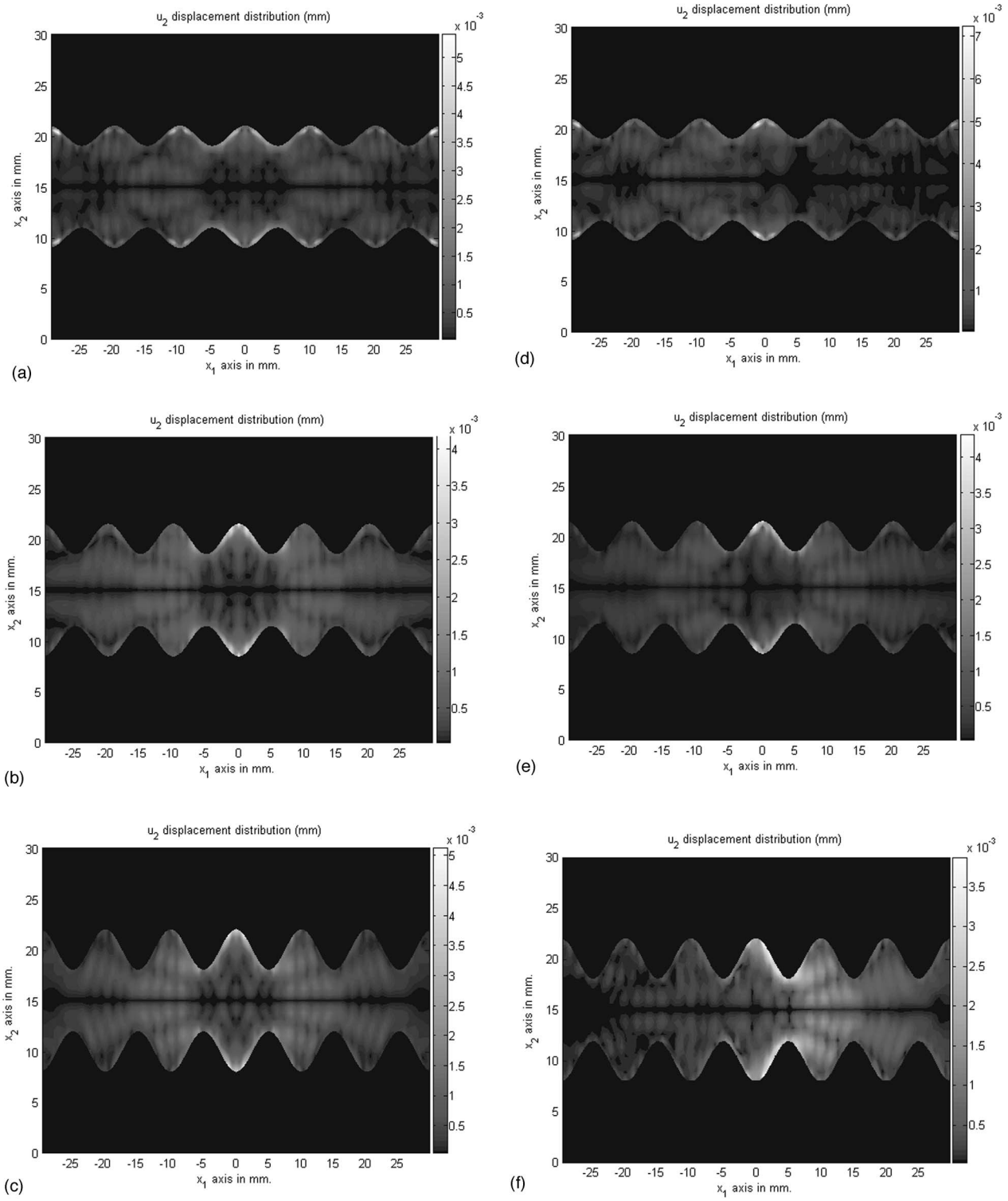

FIG. 5. Vertical displacement fields in three different corrugated waveguides (2, 3, and 4) for two different angles of strike (0° and 30°) (a) in Waveguide 2 for normal incidence, (b) in Waveguide 3 for normal incidence, (c) in Waveguide 4 for normal incidence, (d) in Waveguide 2 for a 30° inclination angle, (e) in Waveguide 3 for a 30° inclination angle, (f) in Waveguide 4 for a 30° inclination angle. As expected, symmetric displacement fields are observed for normal incidence [(a), (b), (c)]. However, for inclined incidence, more energy is observed in the backward direction ($x>0$) in (f) (large corrugation) while the opposite trend is noticed in (e) (small corrugation). Table I gives waveguide dimensions.

the striking beams. In Waveguide 4 [Figs. 4(f) and 5(f)] ultrasonic waves in the waveguide propagate in the backward direction, or, in other words, opposite to the direction of the striking beams. In Waveguide 3 [Figs. 4(e) and 5(e)] the wave propagates in both directions. The phenomenon of the wave propagation in the backward direction in Waveguides 4 and 3 is called "back-propagation." The back-propagation phenomenon can be more clearly seen in Fig. 6. Figure 6 shows amplitudes of u_1 displacement along the central plane of the waveguides. In this figure the displacement variations

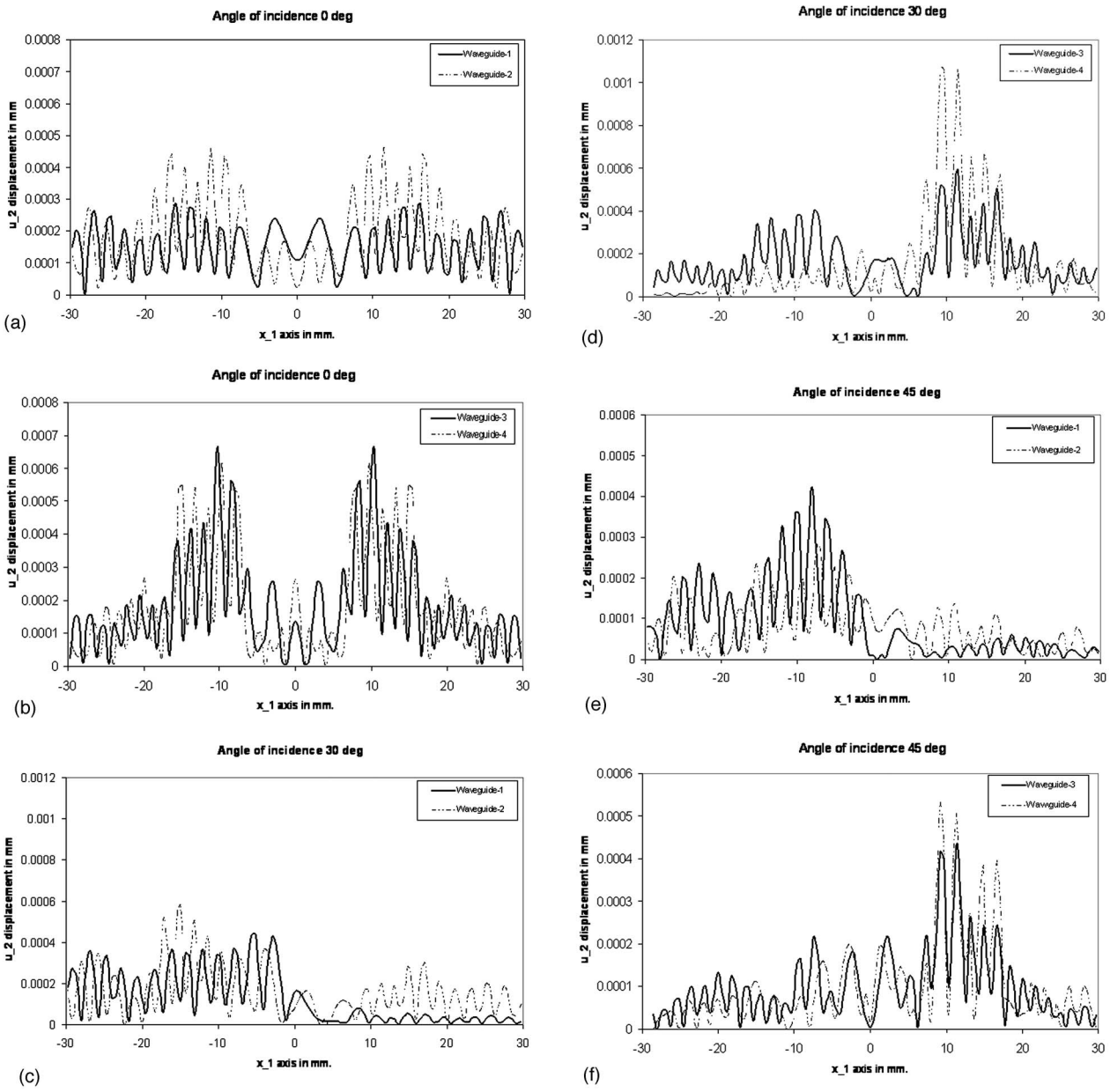

FIG. 6. Vertical displacements at the horizontal central planes of four different corrugated waveguides (dimensions are given in Table I) for three different striking angles (shown in Fig. 3) (a) normal incidence in Waveguides 1 and 2, (b) normal incidence in Waveguides 3 and 4, (c) 30° incidence in Waveguides 1 and 2, (d) 30° incidence in Waveguides 3 and 4, (e) 45° incidence in Waveguides 1 and 2, (f) 45° incidence in waveguides 3 and 4. As expected, (a) and (b) show the symmetric response for normal incidence. For inclined incidence, (c) and (e) show strong wave propagation in the forward direction for small corrugation (Waveguides 1 and 2), while (d) and (f) show strong backward direction wave propagation for large corrugation (Waveguides 3 and 4).

in all four waveguides listed in Table I are shown. These displacement fields are generated for three different transducer orientations, as shown in Fig. 3. Figure 6 clearly shows the back-propagation of ultrasonic waves [Figs. 6(d) and 6(f)] for large corrugation ($\varepsilon/D=0.2$ and 0.15) and forward propagation [Figs. 6(c) and 6(e)] for small corrugation ($\varepsilon/D=0.05$ and 0.1) when the ultrasonic beam strikes the plate at an angle. The ε/D ratio was carefully changed between 0.1 and 0.15 to find out for what value of this ratio the back-propagation starts to dominate. It is found that for the inclined incidence of the ultrasonic bounded beam on a corrugation peak when $\varepsilon/D\approx0.11$ the ultrasonic waves propagate in both directions with almost equal strength. For $\varepsilon/D>0.11$ the back-propagation dominates and for $\varepsilon/D<0.11$ the forward propagation dominates. When the signal frequency in Figs. 4–6 was changed from 1 to 2 MHz, the details of the figures changed to some extent, however, the general conclusion about the forward and backward propagation phenomenon did not change. For 2 MHz plots also (not shown here) it was observed that for $\varepsilon/D>0.11$ the back-propagation dominates and for $\varepsilon/D<0.11$ the forward propagation dominates.

IV. CONCLUSION

Elastic wave propagation in corrugated plates is modeled by the DPSM technique. Displacement mode shapes

generated by DPSM are compared with those obtained analytically. Good qualitative matching between the two sets of mode shapes is obtained. This analysis shows that when bounded acoustic beams strike a corrugated plate at an angle, the elastic waves can propagate in both forward and backward directions in the waveguide depending on the degree of corrugation. The back propagation of ultrasonic waves in corrugated waveguides for large corrugation depth is reported for the first time in this paper.

ACKNOWLEDGMENTS

The authors thank Dr. A. Boström and Dr. A. El-Bahrawy, Chalmers University of Technology, Division of Mechanics, Göteborg, Sweden and Dr. A. K. Mal, University of California, Los Angeles, for sending valuable research material on this subject. This research was partially funded by a grant from the National Science Foundation under Contract No. CMS-9901221.

APPENDIX:

Matrices expressions:

$$\mathbf{DSn}_{TS}=\begin{bmatrix} \mathbf{Gn}_1^1 & \mathbf{Gn}_1^2 & \mathbf{Gn}_1^3 & \cdots & \mathbf{Gn}_1^{M-1} & \mathbf{Gn}_1^M \\ \mathbf{Gn}_2^1 & \mathbf{Gn}_2^2 & \mathbf{Gn}_2^3 & \cdots & \mathbf{Gn}_2^{M-1} & \mathbf{Gn}_2^M \\ \mathbf{Gn}_3^1 & \mathbf{Gn}_3^2 & \mathbf{Gn}_3^3 & \cdots & \mathbf{Gn}_3^{M-1} & \mathbf{Gn}_3^M \\ \cdots & \cdots & \cdots & \cdots & \cdots & \cdots \\ \mathbf{Gn}_{N-1}^1 & \mathbf{Gn}_{N-1}^2 & \mathbf{Gn}_{N-1}^3 & \cdots & \mathbf{Gn}_{N-1}^{M-1} & \mathbf{Gn}_{N-1}^M \\ \mathbf{Gn}_N^1 & \mathbf{Gn}_N^2 & \mathbf{Gn}_N^3 & \cdots & \mathbf{Gn}_N^{M-1} & \mathbf{Gn}_N^M \end{bmatrix}_{(Nx3M)}, \tag{A1}$$

$$\mathbf{S22}'_{TS}=\begin{bmatrix} \mathbf{s}_{22^1}^1 & \mathbf{s}_{22^1}^2 & \mathbf{s}_{22^1}^3 & \mathbf{s}_{22^1}^4 & \mathbf{s}_{22^1}^5 & \cdots & \cdots & \mathbf{s}_{22^1}^{M-2} & \mathbf{s}_{22^1}^{M-1} & \mathbf{s}_{22^1}^M \\ \mathbf{s}_{22^2}^1 & \mathbf{s}_{22^2}^2 & \mathbf{s}_{22^2}^3 & \mathbf{s}_{22^2}^4 & \mathbf{s}_{22^2}^5 & \cdots & \cdots & \mathbf{s}_{22^2}^{M-2} & \mathbf{s}_{22^2}^{M-1} & \mathbf{s}_{22^2}^M \\ \mathbf{s}_{22^3}^1 & \mathbf{s}_{22^3}^2 & \mathbf{s}_{22^3}^3 & \mathbf{s}_{22^3}^4 & \mathbf{s}_{22^3}^5 & \cdots & \cdots & \mathbf{s}_{22^3}^{M-2} & \mathbf{s}_{22^3}^{M-1} & \mathbf{s}_{22^3}^M \\ \cdots & \cdots & \cdots & \cdots & \cdots & \cdots & \cdots & \cdots & \cdots & \cdots \\ \cdots & \cdots & \cdots & \cdots & \cdots & \cdots & \cdots & \cdots & \cdots & \cdots \\ \mathbf{s}_{22^{N-2}}^1 & \mathbf{s}_{22^{N-2}}^2 & \mathbf{s}_{22^{N-2}}^3 & \mathbf{s}_{22^{N-2}}^4 & \mathbf{s}_{22^{N-2}}^5 & \cdots & \cdots & \mathbf{s}_{22^{N-2}}^{M-2} & \mathbf{s}_{22^{N-2}}^{M-1} & \mathbf{s}_{22^{N-2}}^M \\ \mathbf{s}_{22^{N-1}}^1 & \mathbf{s}_{22^{N-1}}^2 & \mathbf{s}_{22^{N-1}}^3 & \mathbf{s}_{22^{N-1}}^4 & \mathbf{s}_{22^{N-1}}^5 & \cdots & \cdots & \mathbf{s}_{22^{N-1}}^{M-2} & \mathbf{s}_{22^{N-1}}^{M-1} & \mathbf{s}_{22^{N-1}}^M \\ \mathbf{s}_{22^N}^1 & \mathbf{s}_{22^N}^2 & \mathbf{s}_{22^N}^3 & \mathbf{s}_{22^N}^4 & \mathbf{s}_{22^N}^5 & \cdots & \cdots & \mathbf{s}_{22^N}^{M-2} & \mathbf{s}_{22^N}^{M-1} & \mathbf{s}_{22^N}^M \end{bmatrix}_{(Nx3M)}, \tag{A2}$$

$$\mathbf{DFn}_{TS}=\begin{bmatrix} g(R_{i1}^1,r_1^1) & g(R_{i1}^2,r_1^2) & g(R_{i1}^3,r_1^3) & \cdots & g(R_{i1}^{M-1},r_1^{M-1}) & g(R_{i1}^M,r_1^M) \\ g(R_{i2}^1,r_2^1) & g(R_{i2}^2,r_2^2) & g(R_{i2}^3,r_2^3) & \cdots & g(R_{i2}^{M-1},r_2^{M-1}) & g(R_{i2}^M,r_2^M) \\ g(R_{i3}^1,r_3^1) & g(R_{i3}^2,r_3^2) & g(R_{i3}^3,r_3^3) & \cdots & g(R_{i3}^{M-1},r_3^{M-1}) & g(R_{i3}^M,r_3^M) \\ g(R_{i4}^1,r_4^1) & g(R_{i4}^2,r_4^2) & g(R_{i4}^3,r_4^3) & \cdots & g(R_{i4}^{M-1},r_4^{M-1}) & g(R_{i4}^M,r_4^M) \\ \cdots & \cdots & \cdots & \cdots & \cdots & \cdots \\ g(R_{iN}^1,r_N^1) & g(R_{iN}^2,r_N^2) & g(R_{iN}^3,r_N^3) & \cdots & g(R_{iN}^{M-1},r_N^{M-1}) & g(R_{iN}^M,r_N^M) \end{bmatrix}_{(NxM)}, \tag{A3}$$

where

$$g(R_{in}^m,r_n^m)=\frac{1}{\rho\omega^2}\left[\left(\frac{1}{r_n^m}ik_fR_{2n}^me^{ik_fr_n^m}-\frac{e^{ik_fr_n^m}}{(r_n^m)^2}R_{2n}^m\right)n_2+\left(\frac{1}{r_n^m}ik_fR_{1n}^me^{ik_fr_n^m}-\frac{e^{ik_fr_n^m}}{(r_n^m)^2}R_{1n}^m\right)n_1\right],$$

$R_{in}^m=(x_{in}^m-y_{in}^m)/r_n^m$ and i take values 1, 2, and 3, except an imaginary quantity.

Ahmad, R., Kundu, T., and Placko, D. (**2003**). "Modeling of the ultrasonic field of two transducers immersed in a homogeneous fluid using distributed point source method," I2M (Instrumentation, Measurement and Metrology) Journal; Vol. **3**, pp. 87–116.

Ahmad, R., Kundu, T., and Placko, D. (**2005**). "Modeling of phased array transducers," J. Acoust. Soc. Am. **117**, 1762–1776.

Banerjee, S. (**2005**). "Elastic wave propagation in corrugated wave guides," PhD dissertation, University of Arizona, Tucson, AZ.

Banerjee, S., and Kundu, T. (**2004**). "Analysis of wave propagation in symmetrically periodic sinusoidal wave-guide," *Health Monitoring and Smart Nondestructive Evaluation of Structural and Biological Systems*, SPIE's 9th Annual International Symposium on NDE for Health Monitoring and Diagnostics, March 15–17, 2004, edited by T. Kundu, San Diego, CA, Vol. **5394**, pp. 89–98.

Banerjee, S., and Kundu, T. (2006a). "Symmetric and anti-symmetric Rayleigh-Lamb modes in sinusoidally corrugated waveguides: An analytical approach," Int. J. Solids Struct. (in press).
Banerjee, S., and Kundu, T. (2006b). "Ultrasonic field modelling in plates immersed in fluids," IEEE Trans. Ultrason. Ferroelectr. Freq. Control (submitted).
Banerjee, S., Kundu, T., and Placko, D. (2006). "Ultrasonic field modelling in multilayered fluid structures using DPSM technique," ASME J. Appl. Mech. (to be published).
Boström, A. (**1983**). "Passbands and stopbands for an electromagnetic waveguide with a periodically varying cross section," IEEE Trans. Microwave Theory Tech. **31**, 752–756.
Boström, A. (**1989**). "Propagating, damped, and leaky surface waves on the corrugated traction-free boundary of an elastic half-space," J. Acoust. Soc. Am. **85**, 1549–1555.
Declercq, N. F., Degrieck, J., Briers, R. and Leory, O. (**2005**). "Diffraction of homogeneous and inhomogeneous plane waves on a doubly corrugated liquid/solid interface," Ultrasonics **43**, 605–618.
El-Bahrawy, A. (**1994a**). "Stopbands and passbands for symmetric Rayleigh-Lamb modes in a plate with corrugated surfaces," J. Sound Vib. **170**(2), 145–160.
El-Bahrawy, A. (**1994b**). "Point force excitation of surface waves along the doubly corrugated traction-free boundary of an elastic half-space," Comm. Div. Mech. **2**.
Fokkemma, J. H. (**1980**). "Reflection and transmission of elastic waves by the spatially periodic interface between two solids (Theory of integral-equation method)," Wave Motion **2**, 375–393.
Glass, N. E., and Maradudin, A. A. (**1983**). "Leaky surface-elastic waves on both flat and strongly corrugated surfaces for isotropic, nondissipative media," J. Appl. Phys. **54**, 796–805.
Hah, Z. G., and Sung, K. M. (**1992**). "Effect of spatial sampling in the calculation of ultrasonic fields generated by piston transducers," J. Acoust. Soc. Am. **92**, 3403–3408.
Harris, G. R. (**1981**). "Review of transient field theory for a baffled planar piston," J. Acoust. Soc. Am. **70**, 10–20.
Ingenito, F., and Cook, B. D. (**1969**). "Theoretical investigation of the integrated optical effort produced by sound field radiated from plane piston transducers," J. Acoust. Soc. Am. **45**, 572–577.
Jensen, J. A., and Svendsen, N. B. (**1992**). "Calculation of pressure fields from arbitrary shaped, apodized, and excited ultrasound transducers," IEEE Trans. Ultrason. Ferroelectr. Freq. Control **39**, 262–267.
Kundu, T. (**2004**). *Ultrasonic Nondestructive Evaluation: Engineering and Biological Material Characterization* (CRC Press, Boca Raton, FL), Chap. 2.
Lee, J. P., Placko, D., Alnuamaini, N., and Kundu, T. (**2002**). "Distributed point source method (DPSM) for modeling ultrasonic fields in homogeneous and non-homogeneous fluid media in presence of an interface," Ecole Normale Superieure de Cachan, France, *1st European Workshop on Structural Health Monitoring*, edited by D. L. Balageas (Pub. DEStech, PA), pp. 414–421.
Lerch, T. P., Schmerr, L. W., and Sedov, A. (**1998**). "Ultrasonic beam models: An edge element approach," J. Acoust. Soc. Am. **104**, 1256–1265.
Lockwood, J. C., and Willette, J. G. (**1973**). "High-speed method for computing the exact solution for the pressure variations in the near field of a baffled piston," J. Acoust. Soc. Am. **53**, 735–741.
Mal, A. K., and Singh, S. J. (**1991**). *Deformation of Elastic Solids* (Prentice–Hall, Englewood Cliffs, NJ).
Morse, P. M., and Ingard, U. K. (**1968**). *Theoretical Acoustics* (McGraw-Hill, New York).
Nayfeh, A. H., and Kandil, O. A. (**1978**). "Propagation waves in cylindrical hard-walled ducts with generally weak undulations," AIAA J. **16**, 1041–1045.
Newberry, B. P., and Thompson, R. B. (**1989**). "A paraxial theory for the propagation of ultrasonic beams in anisotropic solids," J. Acoust. Soc. Am. **85**, 2290–2300.
Placko, D., and Kundu, T. (**2001**). "A theoretical study of magnetic and ultrasonic sensors: Dependence of magnetic potential and acoustic pressure on the sensor geometry," *Advanced NDE for Structural and Biological Health Monitoring, Proceedings of SPIE*, SPIE's 6th Annual International Symposium on NDE for Health Monitoring and Diagnostics, edited by T. Kundu, 4–8 March, Newport Beach, California, Vol. **4335**, pp. 52–62.
Placko, D., and Kundu, T. (**2004**). "Modeling of ultrasonic field by distributed point source method," *Ultrasonic Nondestructive Evaluation: Engineering and Biological Material Characterization*, edited by T. Kundu (CRC Press, Boca Raton, FL), Chap. 2, pp. 144–201.
Placko, D., Kundu, T., and Ahmad, R. (**2002**). "Theoretical computation of acoustic pressure generated by ultrasonic sensors in presence of an interface," *Smart NDE and Health Monitoring of Structural and Biological Systems*, SPIE's 7th Annual International Symposium on NDE and Health Monitoring and Diagnostics, San Diego, CA, Vol. **4702**, pp. 157–168.
Placko, D., Kundu, T., and Ahmad, R. (**2003**). "Ultrasonic field computation in presence of a scatterer of finite dimension," *Smart NDE and Health Monitoring of Structural and Biological Systems*, SPIE's 8th Annual International Symposium on NDE and Health Monitoring and Diagnostics, San Diego, CA, Vol. **5047**, pp. 169–179.
Placko, D., Liebeaux, N., and Kundu, T. (2001). "Presentation d'une method generique pour la modelisation des capteurs de type ultrasons," Magnetiques at Electrostatiques, Instrumentation, Mesure, Metrologie (I2M Journal): Evaluation Nondestructive, Vol. **1**, pp. 101–125.
Rayleigh, L. (**1965**). *Theory of Sound* (Dover, New York), Vol. **II**, pp. 162–169.
Scarano, G., Denisenko, N., Matteucci, M., and Pappalardo, M. (**1985**). "A new approach to the derivation of the impulse response of a rectangular piston," J. Acoust. Soc. Am. **78**, 1109–1113.
Schmerr, L. W. (**1998**). *Fundamental of Ultrasonic Nondestructive Evaluation-A Modeling Approach* (Plenum, New York).
Schmerr, L. W. (**2000**). "A multi-Gaussian ultrasonic beam model for high performance simulations on a personal computer," Mater. Eval. 882–888.
Schmerr, L. W., Kim, H.-J., Huang, R., and Sedov, A. (**2003**). "Multi-Gaussian ultrasonic beam modeling," *Proceedings of the World Congress of Ultrasonics*, WCU 2003, Paris, 7–10 September, **2003**, pp. 93–99.
Sha, K., Yang, J., and Gan, W.-S. (**2003**). "A complex virtual source approach for calculating the diffraction beam field generated by a rectangular planar source," IEEE Trans. Ultrason. Ferroelectr. Freq. Control **50**, 890–895.
Spies, M. (**1994**). "Transducer-modeling in general transversely isotropic media via point-source-synthesis theory," J. Nondestruct. Eval. **13**, 85–99.
Spies, M. (**1995**). "Elastic wave propagation in transversely isotropic media II: the generalized Rayleigh-function and an integral representation for the transducer field theory," J. Acoust. Soc. Am. **97**, 1–13.
Spies, M. (**1999**). 'transducer field modeling in anisotropic media by superposition of Gaussian base functions," J. Acoust. Soc. Am. **105**, 633–638.
Spies, M. (**2004**). "Analytical methods for modeling of ultrasonic nondestructive testing of anisotropic media," Ultrasonics **42**, 213–219.
Standström, S. E. (**1986**). "Stopbanda in a corrugated parallel plate waveguide," J. Acoust. Soc. Am. **79**, 1293–1298.
Standström, S. E. (**1987**). "A comparison of some techniques for corrugated parallel plate wave guides," J. Acoust. Soc. Am. **82**, 1797–1803.
Stepanishen, P. R. (**1971**). "Transient radiation from piston in an infinite planar baffle," J. Acoust. Soc. Am. **49**, 1627–1638.
Waterman, P. C. (**1975**). "Scattering by periodic surfaces," J. Acoust. Soc. Am. **57**, 791–802.
Wen, J. J., and Breazeale, M. A. (**1988**). "A diffraction beam field expressed as the superposition of Gaussian beams," J. Acoust. Soc. Am. **83**, 1752–1756.
Wu, P., Kazys, R., and Stepinski, T. (**1995**). "Analysis of the numerically implemented angular spectrum approach based on the evaluation of two-dimensional acoustic fields. Part I. Errors due to the discrete Fourier transform and discretization," J. Acoust. Soc. Am. **99**, 1139–1148.